International Journal of Robotics and Automation, Vol. 36, 2021

Special Issue: Automatic Detection and Assessment of Bridge Structures

A STRESS DAMAGE ASSESSMENT METHOD OF STEEL BARS IN CONCRETE STRUCTURES BASED ON MMM

Lei Liu,*,** Qianwen Xia,* Ya Li,* and Yinghao Qu*

Abstract

To realize the assessment of the stress damage of the tensile steel bars in concrete structures, a metal magnetic memory (MMM) signals acquisition experiment of the concrete rectangular beams subjected to increasing and decreasing loads was carried out. A new parameter called "difference of deviation rate curve (dDr)" was proposed to evaluate the stress damage of tensile steel bars in the test beams. Experimental results revealed that the change laws of MMM signals did not coincide during the loading and unloading process, and the MMM signals of different specimens deviated to different degrees after unloading. Importantly, the parameter "dDr" successfully realized the stress damage assessment of tensile steel bars in the test beams. The results of this paper can effectively provide a basis for the damage assessment of tensile steel bars in concrete structures.

Key Words

Reinforced concrete structure, tensile steel bars, stress damage, metal magnetic memory, assessment

1. Introduction

With the rapid development of transportation, bridges have a great significance as important nodes of roads. In recent years, many bridge collapse events have been reported, and the structural safety of bridges deserves crucial attention [1]. Health monitoring systems for operational safety monitoring purposes have been set up in a large number of bridges [2]. Structural health monitoring (SHM) is a real-time perception, identification, and evaluation of structural damage and safety states that are executed by means of sensors. The SHM system generally includes various sensors, data acquisition devices, data transmission systems, data management databases, data analysis and modelling modules, state assessment and performance prediction modules, early warning devices, visual user interfaces, and software and operating systems [3]. SHM is widely used in civil, aerospace, and mechanical engineering [4]–[12].

With the continuous improvement of science and technology, strong monitoring and weak diagnosis has become the main form of current SHM systems. To achieve the goal of SHM, it is necessary to increase the accuracy of data processing and health diagnosis by taking the advantages of automatic and online self-diagnostic technologies.

A classic problem in SHM is the identification of damages. Currently, no complete theoretical guidance is available for bridge health monitoring, and no single detection method can provide correct identification results. Current SHM methods mainly work based on vibration shock [13], [14], artificial neural network [15], statistical pattern recognition [16], and signal processing [17], [18]. However, in the structural monitoring of large-scale infrastructure such as large-span bridges, the application of the above concepts has many limitations [19]–[21]. In recent years, a new monitoring method based on metal magnetic memory (MMM) is proposed to monitor the stress damage of tensile steel bars inside bridges [22].

The MMM-based detection technology was first proposed by Doubov. This technology uses the changeable information of the leakage magnetic field on the test piece surface to diagnose whether the ferromagnetic component has defects or stress concentrations. In comparison with other magnetic non-destructive testing technologies, the MMM-based detection method is simple and cost-effective, and it requires no manual excitation. To reveal the mechanism of the MMM technology, Jiles [23] made an in-depth study on the force-magnetic effect of ferromagnetic materials, discussed the relationship among stress, magnetization, and magnetostriction, and established a theoretical model. Ren *et al.* [24] published the first monograph on the MMM technology. Zhou and others [25], [26] used the MMM technology for the rust detection inside concretes, located the rusted area according to the magnetic

* School of Civil Engineering, Chongqing Jiaotong University, Chongqing 400074, P.R. China; email: {50869960, 510310997, 1044486115}@qq.com yhqu@mails.cqjtu.edu.cn

** China Communications Construction Co., Ltd., Beijing 100088, P.R. China

Corresponding author: Yinghao Qu

Recommended by Dr. Jingzhou Xin

(DOI: 10.2316/J.2021.206-0542)

field's change information on the surface of the rusted test piece, and semiquantitatively evaluated the degree of corrosion. The low-frequency magnetic flux leakage detection technology developed by Jiao *et al.* [27] could detect internal and external surface damages of ferromagnetic components. Jin *et al.* [28] proposed a method based on the piezomagnetic effect to monitor the fatigue damage state of reinforced concrete members.

In this article, an MMM signal acquisition experiment of the concrete rectangular beams during the loading and unloading process was carried out. According to the experimental results, a new parameter called "difference of deviation rate curve (dDr)" was proposed to characterize the degree of stress damage of tensile steel bars in the test beams.

2. J-A Theory

Two main physical theories are available on the internal friction of the magnetization process and hysteresis: (i) Preisach model and (ii) Jiles–Atherton (J-A) model. The J-A model was first proposed by Jiles *et al.*, and it is suitable to predict the magnetization of anisotropic ferromagnetic materials. According to the J-A model, the energy loss caused by the irreversible magnetic wall displacement is mainly considered. The original J-A model has been extended to include the magnetization due to hysteresis losses, the magnetization of isotropic materials, and the magnetization of materials under stresses.

The establishment of the J-A magnetization model consists of two parts:

- the establishment of a no-lag magnetization model and
- the quantification of the energy loss due to the irreversible magnetic domain wall effect.

No hysteresis magnetization refers to an ideal magnetization state that can eliminate irreversible magnetization. Based on thermodynamics, Jiles and Atherton established a non-magnetic hysteresis curve by the Langevin relationship:

$$M_{an} = M_s \left[\coth\left(\frac{H}{a}\right) - \frac{a}{H} \right] = f(H), \tag{1}$$

where a is the material planning constant, $a = \frac{\mu_0 m}{k_B T}$; μ_0 is the vacuum permeability ($\mathrm{N/A^2}$), $\mu_0 = 4\pi \times 10^{-7}$; m is the magnetic moment ($\mathrm{A{\cdot}m^2}$); T is the temperature (K); k_B is the Boltzmann constant (J/K), $k_B = 1.3806488 \times 10^{-2}$; and M_s is the saturation magnetization.

When a material is under an external magnetic field in a single direction, the magnetic domain wall produces two types of changes: (i) reversible magnetization – this process mainly occurs due to domain wall bending and is accompanied by the storage and release of the domain wall energy (no energy loss occurs) and (ii) irreversible magnetization – this process mainly occurs due to magnetic domain wall displacement and it is accompanied by energy loss.

Let us assume that the magnetic domains of reversible and irreversible magnetization are m' and m, respectively, then their corresponding angles to the external magnetic field are θ and 0. A pinning effect acts between these two magnetic domains, and the strength of the nailing action depends on two factors: (i) the self-factor of the pinning effect and (ii) the opposite direction of the magnetic domains on both sides. When the magnetic domain magnetization state changes from m' to m, the energy change can be expressed as:

$$\Delta E = \mu_0 m \cdot H - \mu_0 m' \cdot H. \tag{2}$$

The energy loss caused by the moving distance x of the magnetic domain wall in area A is:

$$E_{pin} = \int_0^x n \left(\frac{1}{2} \mu_0 < \varepsilon_\pi > (1 - \cos\theta) \right) A dx, \tag{3}$$

where n is the pinning density. The irreversible magnetization change of the ferromagnetic material caused by the movement of the magnetic domain wall can be expressed as:

$$dM_{irr} = m(1 - \cos\theta) A dx. \tag{4}$$

Under the action of an external magnetic field, the ferromagnetic material becomes magnetized, exhibits magnetism to the outside, and generates a magnetic field around it. The generated magnetic field also adversely affects the magnetization state of the ferromagnetic material, and this phenomenon is known as the self-coupling of ferromagnetic materials. Therefore, a truly effective magnetic field (H_e) should be superimposed on the external magnetic field by a coupling field of intensity αM (α is the coupling coefficient), which can be expressed as:

$$H_e = H + \alpha M. \tag{5}$$

The magnetization energy of a ferromagnetic material is equal to the non-lag magnetization energy minus the energy loss. The energy balance equation can be expressed as:

$$\mu_0 \int M_{irr} dH_e = \mu_0 \int M_{an} dH_e - \mu_0 k \int \frac{dM_{irr}}{dM_e} dH_e. \tag{6}$$

Now, the simultaneous differentiation on both sides of (6) results in the following equation:

$$M_{irr} = M_{an} - k\delta \frac{dM_{irr}}{dH_e}, \tag{7}$$

where δ represents the directional change of the external magnetic field, $\delta \pm 1$. When $\frac{dH}{dt} > 0$, $\delta = 1$ and when $\frac{dH}{dt} < 0$, $\delta = -1$. The reversible magnetization (M_{rev}) can be expressed as:

$$M_{rev} = c(M_{an} - M_{irr}), \tag{8}$$

where c is the magnetic domain wall bending constant.

The total magnetization M can be divided into two parts: (i) the reversible magnetization (M_{rev}) caused by

Table 1
Reinforcement Information 12 Pieces of Test Beam

Number	Reinforcement Information		
	Tensile Steel Bars	Compression Steel Bars	Stirrup
B1 B2 B3	Two deformed bars of HPB235 with a diameter of 8 mm	No compression steel bars in the pure bending section	No stirrups in the pure bending section
B4 B5 B6	Two deformed bars of HPB235 with a diameter of 8 mm	Two deformed bars of HPB235 with a diameter of 8 mm	One deformed bar with a diameter of 8 mm and model HPB235. Stirrup spacing 100 mm
B7 B8 B9	Two deformed bars of HPB235 with a diameter of 12 mm	No compression steel bars in the pure bending section	No stirrups in the pure bending section
B10 B11 B12	Two deformed bars of HPB235 with a diameter of 12 mm	Two deformed bars of HPB235 with a diameter of 8 mm	One deformed bar with a diameter of 8 mm and model HPB235. Stirrup spacing 100 mm

the magnetic domain wall bending and (ii) the irreversible magnetization (M_{irr}) caused by magnetic domain wall displacement:

$$M = M_{rev} + M_{irr}. \tag{9}$$

The focus of the present article is to obtain the following two important information based on the Jiles–Atherton model and related experiments:

- The periodic stress causes the magnetization of a ferromagnetic material to evolve irreversibly. Therefore, the magnetization cannot recover after the ferromagnetic material returns to the initial state, which causes MMM signal changes.
- Plastic deformation generates microcracks and micropores inside the material. The microcracks and micropores act as crystal defects to cause local magnetization, which hinders material magnetization (the plastic deformation concentrated area become internal magnetic source) and causes outward scattering, and eventually leads to the MMM phenomenon.

3. Experimental Process and Analysis

3.1 Production of Test Pieces

Based on the earlier theoretical analysis, it is theoretically feasible to monitor the stress damage of tensile steel bars of reinforced concrete structures. For practical verification, an MMM signal acquisition experiment of 12 pieces of concrete test beams was carried out during loading and unloading. In the experiment, 12 pieces of C40 concrete beams with a size of 100 mm × 200 mm × 1,850 mm were prefabricated. As shown in Table 1, the test beams were divided into four categories according to the different reinforcement methods. For each type of reinforcement concrete, three pieces were prepared. The thickness of the concrete protective layer was 25 mm, and the stirrup was Φ8 at 100 (stirrup diameter = 8 mm and spacing = 100 mm) single limb hoops. The schematic map and reinforcement diagram of the experimental reinforced concrete beam are shown in Fig. 1. The dashed line in Fig. 1 indicates that there were or were not steel bars in the pure bending section.

3.2 Loading and Unloading Monitoring Test

3.2.1 "Four-Point Bending" Loading and Unloading

After the curing of the test beams, the MMM signals monitoring was carried out on 12 test beams. The loading method called four-point bending was executed. Four-point bending tests are commonly used to measure the bending properties of materials or structures. The middle position of two loading points was the pure bending section and it was not affected by the shear force. A Honeywell HMR2300 magnetic flux acquisition sensor with an accuracy of 70 micro-Gauss was used to acquire magnetic signals. The layout of the test beam during loading was presented in Fig. 2.

If any of the following phenomena occurs, it was considered that the test beam had reached the ultimate bearing capacity; then, the loading process was stopped and unloading process started.

- The main ribs are pulled.
- The maximum vertical crack width of the tensioned steel bars is 1.5 mm.
- The deflection reaches 1/50 of the span.
- The concrete in the compression zone is crushed.

In the experiment, the steel bars were continuously loaded to reach the ultimate bearing capacity and then unloaded until the external load of the test beam became zero. Simultaneously, the MMM signals of the reinforced concrete test beam were continuously collected. The test beams' loads were measured by a strain gauge, and the ultimate bending moment was obtained.

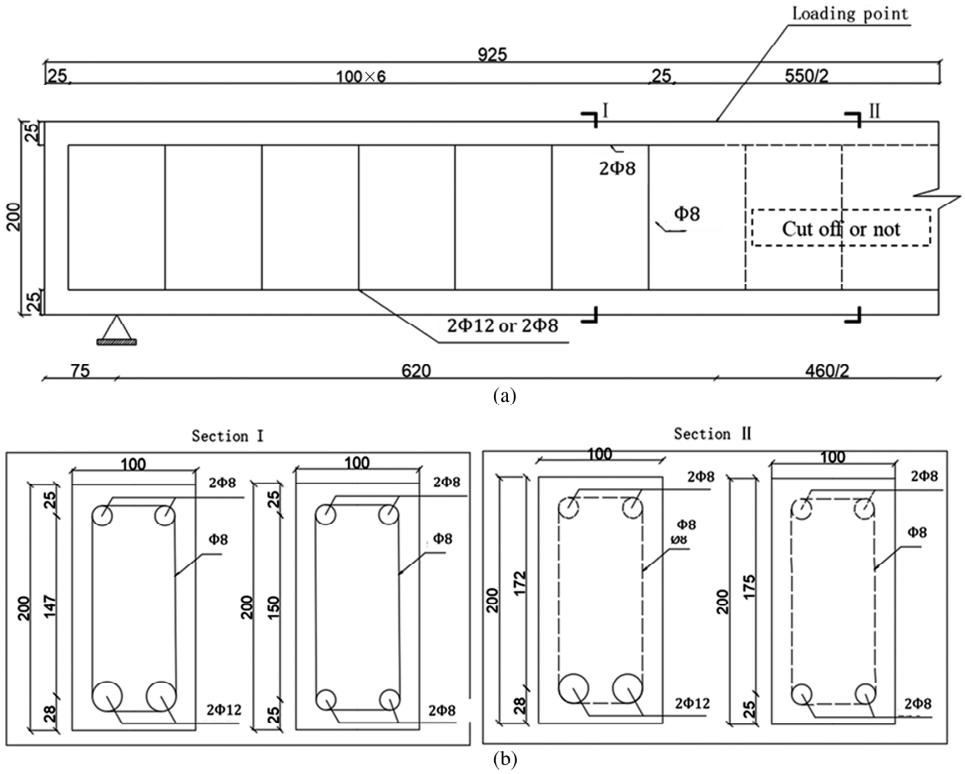

Figure 1. Diagrams of the reinforced concrete test beams (unit: mm): (a) elevation drawing and (b) sectional drawing.

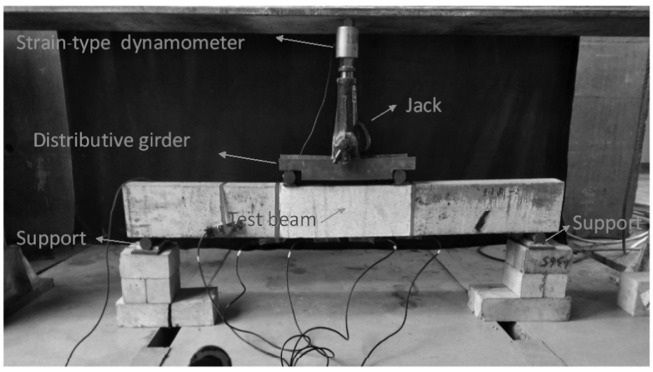

Figure 2. The layout of four-point bending load test.

3.2.2 Measuring Point Arrangement

In this experiment, five measuring points, numbered as 01–05, were selected to monitor MMM signals and the unloading process. Among them, four measuring points were located directly below the tensile reinforcement at the bottom of the beam, and one measuring point was located at the position at the web of beam, as shown in Fig. 3.

4. Test Results and Analysis

The dynamometer strain curves of 12 pieces of test beams during the loading and unloading process were studied. Besides, the MMM signal monitoring data of five measuring points on each test beam were obtained. The ultimate bearing capacity of the test beam was calculated by the dynamometer strain curve of the entire loading and unloading process.

It should be noted that the obtained MMM signal data at each measuring point included three magnetic components of B_x, B_y, and B_z. By comparing and analysing the B_x, B_y, and B_z curves of each test beam, the B_x component could be used to avoid the influence of the pure curved stirrups. Therefore, the B_x component that was in the direction of longitudinal tensile reinforcement was selected for the analysis.

4.1 Ultimate Bearing Capacity Test Result

During the loading process, vertical cracks occurred, as shown in Fig. 4. From the development form of the cracks in the figure, it could be seen that it was a typical damage of the under-reinforced beam. After loading, the ultimate bearing capacities (M_u) of all test beams were listed in Table 2. It is evident that the same type of test beams had a similar ultimate bearing capacity without a large dispersion, and the result is reliable.

4.2 B_x Component Monitoring Results

The variations of the B_x curves of the 12 test beams monitored during the entire loading and unloading process were almost the same. Hence, only the B_x curves of the beams B1, B4, B8, and B11 were given to describe the experimental results. The relationship curves of B_x and bending moments (M) are shown in Fig. 5.

In Fig. 5, MMM signals B_x were sensitive to changes of M. The results obtained by the four types of beams were basically similar. Further analysis showed that the change law of B_x during the loading process did not coincide with the unloading process. The reason for the

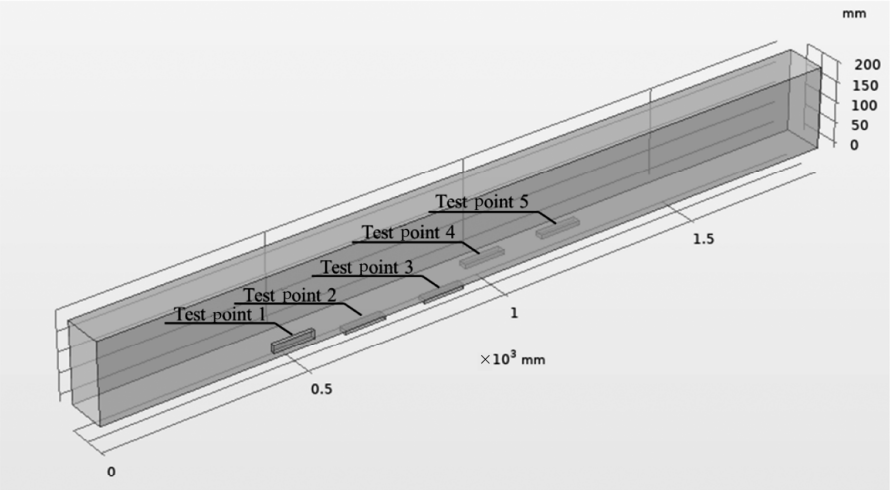

Figure 3. Layout of magnetic moment monitoring measuring points (Strain-type dynamometer).

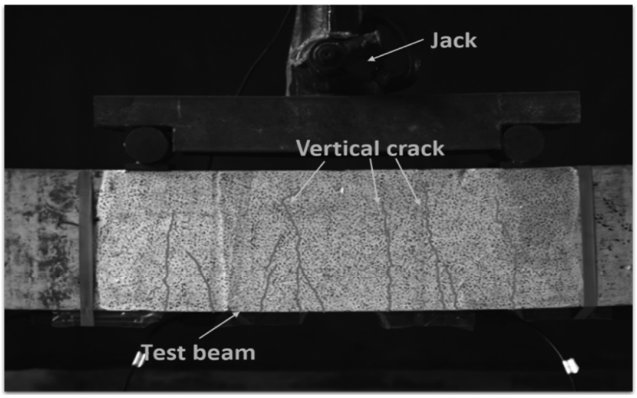

Figure 4. Crack development in the 8-D-1 test beam.

Table 2
Ultimate Bearing Capacities (M_u) of 12 Test Beams

Lable	B1	B2	B3
M_u/kN·m	9.18	9.69	10.02
Lable	B4	B5	B6
M_u/kN·m	11.24	10.71	10.71
Lable	B7	B8	B9
M_u/kN·m	19.46	18.89	18.25
Lable	B10	B11	B12
M_u/kN·m	18.43	18.96	19.81

above phenomenon was that the loading process include not only the elastic deformation but also the microscopic plastic damage. In the unloading process, it was mainly manifested as elastic deformation. During the loading process, due to the microscopic plastic damage, the changes of the magnetic domains were constrained, thus affecting the change of magnetization. Therefore, in the macroscopic view, the loading and unloading path could not be repeated. Moreover, the non-coincidence of the B_x signals from the loading start point and the unloading end point could also reflect the impact of microplastic damage on the MMM signals. Therefore, the degree of deviation of the MMM signals after loading and unloading could be used to qualitatively characterize the stress damage of reinforced concrete.

4.3 Stress Damage Classification Criterion

The B_x curves from the loading phase to the unloading phase at the same load (stress) level were extracted, and the "deviation rate curves" were plotted based on the B_x values in the loading phase. The stress damage of the tensile steel bars inside the test beam was evaluated based on the "deviation rate curves".

The extraction of a "deviation rate curves" was carried out in two steps: (1) determination of a load (stress) level and (2) calculation of the "deviation rate curves" corresponding to the loaded into the unloading interval at the load (stress) level.

Considering that the load (stress) level of the self-weight in the actual reinforced concrete beam bridge was slightly higher (0.5 times) than the limit load (stress), 0.5 times of fold ultimate load (stress) was selected as the reference to plot "deviation rate curves":

$$Dr = \frac{B - B_{0.5L}}{B_{0.5L}} \tag{10}$$

where B refers to the value of any B_x signal in the loading and unloading interval corresponding to 0.5 times of the ultimate load and $B_{0.5L}$ is the value of any B_x signal loaded to 0.5 times of the ultimate load. Due to space limitation, the "deviation rate curves" of four test beams are plotted in Fig. 6.

Because only the sensors numbered 02–05 were placed at the bottom of the test beam, the Dr data of sensors numbered 02–05 were used to evaluate the stress damage of the steel bars later. In addition, combined with the

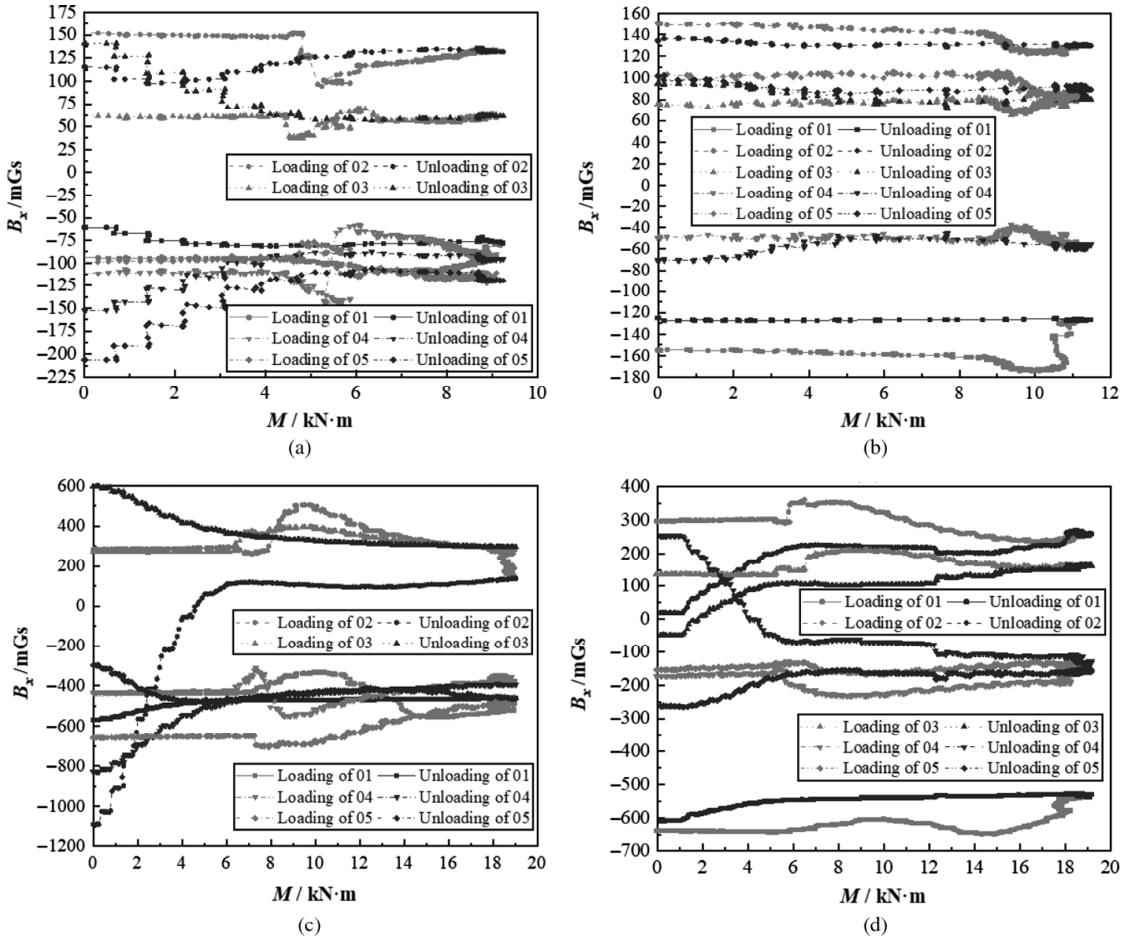

Figure 5. Change laws of B_x signal with the bending moment at all measuring points of test beams: (a) B1 test beam; (b) B4 test beam; (c) B8 test beam; and (d) B11 test beam.

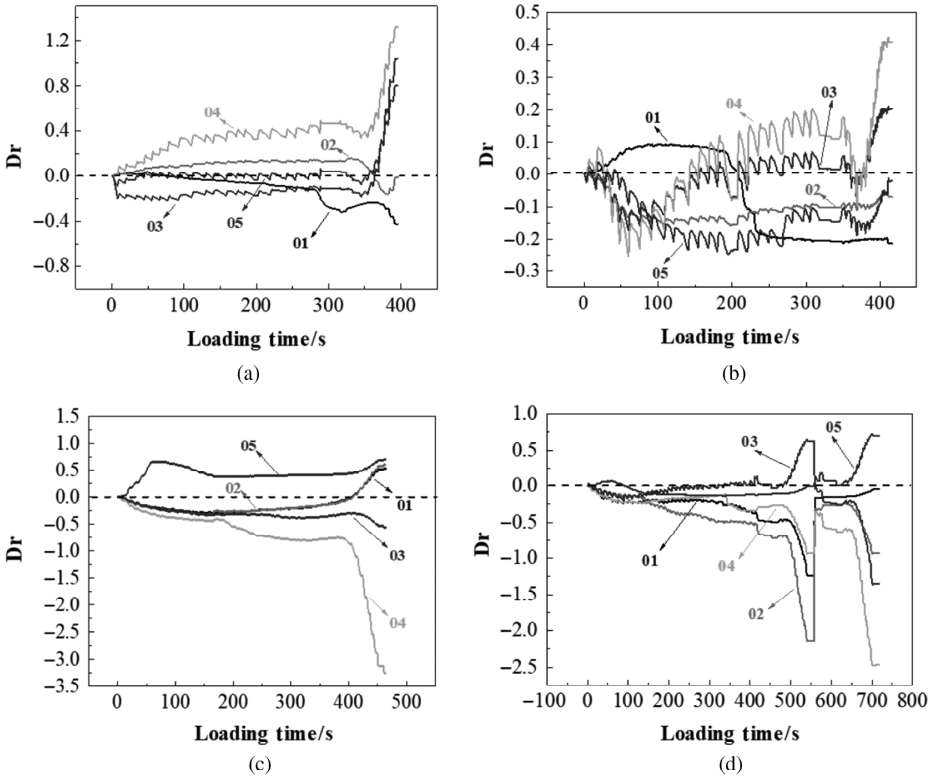

Figure 6. The "deviation rate curves" of all measuring points of four test beams: (a) B1 test beam; (b) B4 test beam; (c) B8 test beam; and (d) B11 test beam.

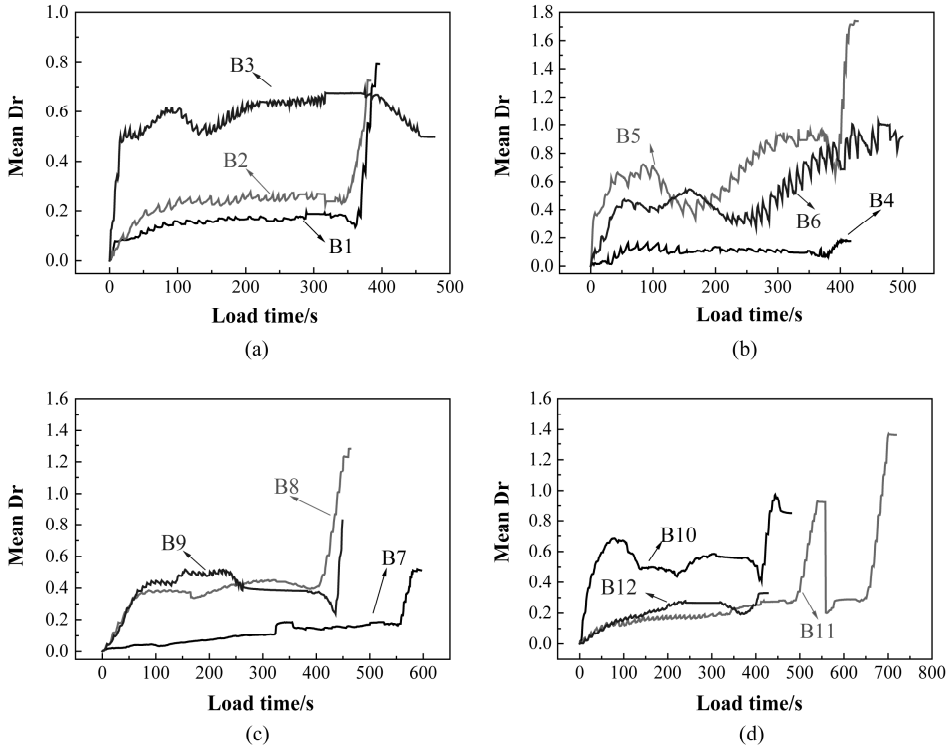

Figure 7. "Mean deviation rate curves" of all test beams: (a) B1, B2, and B3 test beams; (b) B4, B5, and B6 test beams; (c) B7, B8, and B9 test beams; and (d) B10, B11, and B12 test beams.

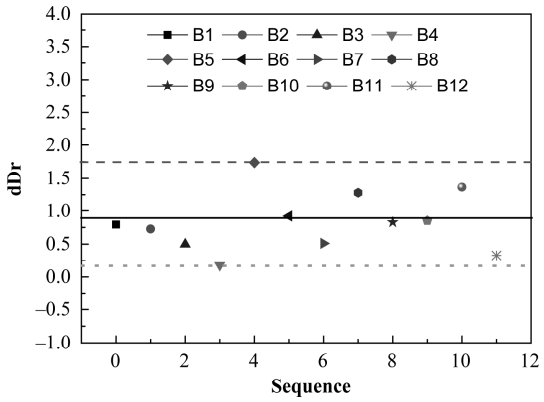

Figure 8. The dDr values of all test beams.

actual engineering situation, considering the difference in the working conditions corresponding to the data measured by the four sensors in the pure curved section, that is, the stress values of the different measuring points caused by the concrete cracking should be different. However, considering that the range of pure bending was not large and no concrete fracture occurred at dense cracks and pure bends, a small difference was noticed between the experimental results of different measured points.

Therefore, the mean value curves of the "deviation rate curves" corresponding to the four sensors numbered 02–05 in the pure curved section were taken as the "deviation rate curves" of each test beam. The "mean deviation rate curves" at 0.5 times of ultimate load (stress) for all 12 test beams are displayed in Fig. 7.

Although the "deviation rate curves" shown in Fig. 7 did not occur with perfect regularity, the following three important information could still be found:

1. The change of the deviation rate curve mainly manifests in two forms: (i) monotonously increased and (ii) first increased and then decreased.
2. The final values of the curves deviated from the initial zero points to varying degrees.
3. The deviation rates (Dr) of all test beams ranged between 0 and 1.8, and it indicated that the MMM signals caused by the stress had a certain range and can be quantified.

The deviation of the final values of the curves from the initial zero point mainly occurred due to stress damage. Therefore, the differences between the final values of the "deviation rate curves" and the initial zero value, called dDr, could be extracted to qualitatively evaluate the stress damage. The dDr values of all 12 test beams are summarized in Fig. 8.

It is noticeable from Fig. 8 that the dDr values of all test beams fluctuated within the range of 0.17–1.74. According to the distribution of dDr values, three lines could be drawn: minimum line (dashed line), mean line (solid line), and the largest line (dotted line).

When the dDr value is close to the dotted line, the stress damage degree of the test beam is low, which indicates that the bridge can be used normally in reality, and only routine maintenance is required.

When the dDr value was close to the solid line, the stress damage degree of the beam bridge was large, which indicates that the bridge is approaching the limit use condition in reality, and has serious problems. Therefore, special inspections are needed depending on the actual situation.

When the dDr value is close to the dashed line, the stress damage degree of beam bridge is very large, which indicates that the bridge has reached the limit use condition in reality, and may collapse at any time. It is necessary to immediately prohibit the passage or construction to ensure the safety of personnel.

Therefore, the dDr can be used to realize the assessment of stress damage and early warning monitoring of bridges.

5. Conclusion

In this article, the reinforced concrete beams were loaded and then unloaded. The corresponding MMM signals are collected. The main conclusions are described as follows:

1. The theoretical analysis based on the classical Jiles–Atherton magnetic-force coupling model expressed that it was feasible to apply MMM signals to monitor the stress damage of tensile steel bars in concrete bridges.
2. The loading and unloading paths of the B_x monitoring curves of all 12 test beams did not coincide, and the B_x signals of the loading start point and unloading end point were deviated. The reason for the phenomenon was due to the microplastic damages during the loading and unloading process.
3. A parameter called dDr was proposed and it could qualitatively evaluate the degree of stress damage of tensile steel bars.

Acknowledgement

This research was financially supported by Science and Technology Support Plan of Guizhou Province ([2018] 2154) and the Postgraduate Education Innovation Fund of Chongqing Jiaotong University (2019S0158).

References

[1] J.Y. Yang, B.H. Xia, Z. Chen, *et al.*, Vibration-based structural damage identification: A review, *International Journal of Robotics and Automation*, *35*(2), 2020, 123–131.

[2] Z. Chen, X. Zhou, X. Wang, *et al.*, Deployment of a smart structural health monitoring system for long-span arch bridges: A review and a case study, *Sensors*, *17*(9), 2017, 2151.

[3] Y.Q. Bao, Z.C. Chen, S.Y. Wei, *et al.*, The state of the art of data science and engineering in structural health monitoring, *Engineering*, *5*(2), 2019, 234–242.

[4] H. Li, J.P. Ou, X.G. Zhang, *et al.*, Research and practice of health monitoring for long-span bridges in the mainland of China, *Smart Structures & Systems*, *15*(3), 2015, 555–576.

[5] J.P. Ou and H. Li, Structural health monitoring in mainland China: Review and future trends, *Structural Health Monitoring*, *9*(3), 2010, 219–231.

[6] B.F. Spencer, M.E. Ruiz-Sandoval, and N. Kurata, Smart sensing technology: Opportunities and challenges, *Structural Control & Health Monitoring*, *11*(4), 2010, 349–368.

[7] H. Wang, T.Y. Tao, A.Q. Li, and Y.F. Zhang, Structural health monitoring system for Sutong cable-stayed bridge, *Smart Structures & Systems*, *18*(2), 2016, 317–334.

[8] P.C. Chang, A. Flatau, and S.C. Liu, Health monitoring of civil infrastructure, *Structural Health Monitoring*, *2*(3), 2003, 257–267.

[9] A.A. Mufti, Structural health monitoring of innovative Canadian civil engineering structures, *Structural Health Monitoring*, *1*(1), 2002, 89–103.

[10] J.M. Ko and Y.Q. Ni, Technology developments in structural health monitoring of large-scale bridges, *Engineering Structures*, *27*(12), 2005, 1715–1725.

[11] X.H. He, X.G. Hua, Z.Q. Chen, and F.L. Huang, EMD-based random decrement technique for modal parameter identification of an existing railway bridge, *Engineering Structures*, *33*(4), 2011, 1348–1356.

[12] X.H. He, J. Fang, A. Scanlon, and Z.Q. Chen, Wavelet-based nonstationary wind speed model in Dongting Lake cable-stayed bridge, *Engineering*, *2*(11), 2010, 895–903.

[13] H. Chen, M. Kurt, Y.S. Lee, *et al.*, Experimental system identification of the dynamics of a vibro-impact beam with a view towards structural health monitoring and damage detection, *Mechanical Systems & Signal Processing*, *46*(1), 2014, 91–113.

[14] Z. Ismail, H. Abdul Razak, and A.G. Abdul Rahman, Determination of damage location in RC beams using mode shape derivatives, *Engineering Structures*, *28*(11), 2006, 1566–1573.

[15] F. Abbassi, T. Belhadj, S. Mistou, and A. Zghal, Parameter identification of a mechanical ductile damage using artificial neural networks in sheet metal forming, *Materials Design*, *45*, 2013, 605–615.

[16] R. Yao and S.N. Pakzad, Autoregressive statistical pattern recognition algorithms for damage detection in civil structures, *Mechanical Systems & Signal Processing*, *31*, 2012, 355–368.

[17] A. Kunwar, R. Jha, M. Whelan, and K. Janoyan, Damage detection in an experimental bridge model using Hilbert–Huang transform of transient vibrations, *Structural Control & Health Monitoring*, *20*(1), 2013, 1–15.

[18] S.S. Patel, A.P. Chourasia, S.K. Panigrahi, *et al.*, Damage identification of RC structures using wavelet transformation, *Procedia Engineering*, *144*, 2016, 336–342.

[19] S.W. Doebling, C.R. Farrar, M.B. Prime, *et al.*, *Damage identification and health monitoring of structural and mechanical systems from changes in their vibration characteristics: A literature review*, 1st ed. (New Mexico: Los Alamos National Laboratory Press, 1996).

[20] K.C. Chang and C.W. Kim, Modal-parameter identification and vibration-based damage detection of a damaged steel truss bridge, *Engineering Structures*, *122*, 2016, 156–173.

[21] R.V. Farahani and D. Penumadu, Damage identification of a full-scale five-girder bridge using time-series analysis of vibration data, *Engineering Structures*, *115*, 2016, 129–139.

[22] H. Zhang, J.T. Zhou, R.Q. Zhao, *et al.*, Experimental study on detection of rebar corrosion in concrete based on metal magnetic memory, *International Journal of Robotics and Automation*, *32*(5), 2017, 530–537.

[23] D.C. Jiles, Theory of the magnetomechanical effect, *Journal of Physics D-Applied physics*, *28*(8), 1995, 1537–1546.

[24] J.L. Ren, M.J. Lin, Y.B. Chi, *et al.*, *Metal magnetic memory detection technology,* 1st ed. (Beijing: China Electric Power Press, 2000).

[25] J.T. Zhou, J.L. Qiu, Y.X. Zhou, *et al.*, Experimental study on residual bending strength of corroded reinforced concrete beam based on micromagnetic sensor, *Sensors*, *18*(8), 2018, 2635.

[26] R.C. Xia, J.T. Zhou, H. Zhang, *et al.*, Quantitative study on corrosion of steel strands based on self-magnetic flux leakage, *Sensors*, *18*(5), 2018, 1396.

[27] J.P. Jiao, Y. Chang, G.H. Li, *et al.*, Study on low frequency magnetic flux leakage detection technology for internal and external surface cracks of ferromagnetic components, *Chinese journal of instrumentation*, *37*(8), 2016, 1808–1817.

[28] W.L. Jin, J. Zhang, C.S. Chen, *et al.*, A new method for fatigue study of reinforced concrete structures based on piezomagnetism, *Journal of Building Structures*, *37*(4), 2016, 133–142.

Biographies

Lei Liu is currently a doctoral candidate in Chongqing Jiaotong University, Chongqing, China. His current research direction is bridge damage detection and reinforcement.

Qianwen Xia was born in 1994. He is currently studying a master's degree in Bridge and Tunnel Engineering at Chongqing Jiaotong University. His current research is nondestructive testing of bridges.

Ya Li was born in 1996. She received her bachelor's degree in Bridge Engineering in 2018. She is currently studying a master's degree in Bridge and Tunnel Engineering at Chongqing Jiaotong University. Her current research includes bridge engineering and magnetic memory testing.

Yinghao Qu was born in 1994. He is currently studying as a doctoral candidate in Chongqing Jiaotong University. His research direction is bridge damage detection and reinforcement.